

The structural properties of the multi-layer graphene/4H-SiC(0001) system as determined by Surface X-ray Diffraction

J. Hass,¹ R. Feng,¹ J.E. Millán-Otoya,¹ X. Li,¹ M. Sprinkle,¹
P. N. First,¹ C. Berger,^{1,2} W. A. de Heer,¹ and E. H. Conrad¹

¹*The Georgia Institute of Technology, Atlanta, Georgia 30332-0430, USA*

²*Institut Néel, BP166, 38042 Grenoble Cedex, France*

We present a structural analysis of the multi-layer graphene-4HSiC(0001) system using Surface X-Ray Reflectivity. We show for the first time that graphene films grown on the C-terminated (0001) surface have a graphene-substrate bond length that is very short (1.62Å). The measured distance rules out a weak Van der Waals interaction to the substrate and instead indicates a strong bond between the first graphene layer and the bulk as predicted by *ab-initio* calculations. The measurements also indicate that multi-layer graphene grows in a near turbostratic mode on this surface. This result may explain the lack of a broken graphene symmetry inferred from conduction measurements on this system [C. Berger et al., *Science* **312**, 1191 (2006)].

PACS numbers: 61.10.Kw, 68.55.-a, 68.35.-p, 61.46.-w, 61.10.Nz

Keywords: Graphene, Graphite, X-ray reflectivity, X-ray diffraction, SiC, Silicon carbide, Graphite thin film

INTRODUCTION

Recent experiments have demonstrated the unique electronic properties of graphene sheets.[1, 2, 3, 4, 5] These works point to a potential route to a new nanoelectronics paradigm based on an epitaxial graphene (EG) [1]. For the purpose of this paper we define graphene as a single honeycomb layer of graphite regardless of stacking order. At the moment graphene is prepared either by mechanical exfoliation of flakes from a bulk graphite sample that are subsequently deposited on an insulating substrate[2, 3, 4] or by sublimating Si from either of the polar faces of SiC; a process that leaves a small number of graphene layers on the SiC surface.[1] In the latter system, transport measurements infer that the measured high mobilities are limited to just a few graphene layers (perhaps only one), that must lie near the SiC substrate. While there are similarities between the magnetotransport properties of exfoliated graphene and SiC-grown multi-layer graphene films, there are significant differences.[5] For instance graphene layers grown on different polar faces of SiC have electron mobilities that differ by an order of magnitude.[6] Such graphene/substrate specific transport properties strongly suggest that the substrate interaction influences the electronic properties of the graphene sheet. While this simple assertion may seem obvious, the structure and influence of the interface remain points of heated conjecture. One can ask if either the exfoliated or the SiC-grown multi-layer graphene (or both) are really electronically the same as a ideally isolated graphene sheet. In other words, how does the interface in both systems influence their electronic properties? In spite of this debate there has been no direct structural characterization of either the graphene-substrate inter-

face or the graphene layers themselves in either system. In this work we begin to address this problem by performing a detailed investigation of the interface structure of multi-layer graphene grown on the 4H-SiC(0001) surface using Surface X-ray Diffraction (SXD).

Prior investigations of 6H- and 4H-SiC(0001) and (0001) surfaces showed that multi-layer graphene films can be grown on these surfaces by sublimating Si from SiC during heating above $\sim 1200^{\circ}\text{C}$ in ultrahigh vacuum (UHV).[7, 8, 9] These studies show that multi-layer graphene grows epitaxially on the (0001) Si-terminated (Si-face) surface of SiC, while multi-layer graphene grown on the C-terminated (0001) (C-face) surface is rotationally disordered and under some conditions form nanocaps instead of a smooth film.[10] An explanation for the structural differences for films grown on the two different faces was proposed by Forbeaux et al.[8] Their conjecture is that C-face multi-layer graphene becomes polycrystalline because they have a stronger substrate-film bond compared to Si-face graphite. The relative bond strengths were inferred from K-Resolved Inverse Photoemission Spectroscopy (KRIPIES),[8] and High Resolution Electron Energy Loss Spectroscopy (HREELS) measurements.[11] However, recent work has shown that the C-face multi-layer graphene is not polycrystalline and can be grown with domain sizes much larger than those grown on the Si-face.[6] The improved structural order of C-face films correlates with magnetotransport measurements that to date find an order of magnitude improvement in electron mobilities for films grown on the C-face compared to Si-face films.[6] Also, electronic coherence lengths exceeding $1\ \mu\text{m}$ have been measured for multi-layer graphene films prepared on the C-face of SiC.[5] The question becomes: how can a strongly bonded C-

face film seemingly ignore any substrate registry potentials and give rise to large free rotating films?

Besides the question of topography differences, there are more fundamental questions related to electron transport in these films. For instance, how does charge transfer from the substrate contribute to the doping of graphene near the surface? One of the most important questions, and possibly related to the charge transport question, is why transport measurements on multi-layer graphene films grown on the $(000\bar{1})$ C-face seem to be confined to just a few layers? Perhaps the most important question is why conduction measurements suggest the existence of a Berry's phase in three or more graphene layers.[5] Similarly, transport measurement infer[5], and Angle Resolved Photoemission measurements (ARPES) confirm[12], the existence of a Dirac Cone in the band structure of multi-layer graphene films. These effects are not expected to occur in multi-layer graphene system with bulk graphite $AB..$ stacking.[13, 14] In other words, experiments suggests that the major conductor is either an isolated single graphene sheet or possible $AA..$ stacked graphene layers.

In this paper we begin to address these questions. We have performed x-ray reflectivity experiments on the structure of multi-layer graphene grown on the 4H-SiC($000\bar{1}$) surface. We find that the first layer of carbon with an areal density of graphene sits very close to the last bulk SiC layer. For the C-face the graphene-bulk spacing is found to be $1.62 \pm 0.08\text{\AA}$. This number is consistent with recent *ab-initio* calculations that also indicate a covalently bonded first layer that is insulating and has no graphitic electronic character.[15] We also demonstrate that the C-face graphene films are flat with little or no corrugation in contrast with mechanically exfoliated graphite.[16] Also, by analyzing the graphite inter-layer spacing, we can deduce that the graphene sheets are stacked in a way resembling turbostratic graphite.

These results show that films grown on the C-face of SiC have a strongly bonded very flat "buffer" layer. Subsequent graphene layers can be rotationally disordered because of the weak registry forces to this buffer layer. Thus the strong bonding and rotational disorder observed can be reconciled in a simple structural model. Most important, the rotational disorder and turbostratic character of the graphite suggest that the $AB..$ symmetry of the graphite is broken leaving a graphene character to the films that may help to explain their conduction properties.

EXPERIMENTAL

All substrates were 4H-SiC purchased from Cree, Inc.[17] Prior to graphitization the $3 \times 4 \times 0.5\text{mm}$ samples were ultrasonically cleaned in acetone and ethanol. Some samples were hydrogen-etched prior to graphiti-

zation while others were not. The etching removed all surface scratches and left a regularly stepped surface but the graphite quality between etched and non-etched samples is difficult to distinguish.[6] Due to the difficulty of preparing C-face 4H-SiC samples in UHV, they were prepared by heating to 1430°C in a vacuum RF-induction furnace ($P = 3 \times 10^{-5}\text{ Torr}$) for 5–8 min.[6] These parameters produced graphitic films of 4–13 graphene layers. The thicker films grown on the C-face reflects the current difficulty in producing less than 6 graphene layers in a furnace grown environment.[6] Regardless of the film thickness, the interface and multi-layer graphene film parameters measured were consistent as discussed in the next sections. Once samples have been graphitized, they remain inert allowing them to be transported into the Ultra High Vacuum (UHV) chamber. The x-ray scattering experiments were performed at the Advanced Photon Source, Argonne National Laboratory, on the 6IDC- μ CAT UHV ($P < 2 \times 10^{-10}\text{ Torr}$) beam line at 16.2 keV photon energy.

For all samples the number of graphene layers present was determined by measuring the x-ray intensity as a function of ℓ along the graphite $(1, \bar{1}, \ell)_G$ rod.[9] The notation $(h, k, \ell)_G$ identifies a reciprocal-space point in reciprocal units (*r.l.u.*) of the standard graphite hexagonal reciprocal lattice basis vectors $\mathbf{q} = (ha_G^*, kb_G^*, \ell c_G^*)$, where $a_G^* = b_G^* = 2\pi/(a_G\sqrt{3}/2)$ and $c_G^* = 2\pi/c_G$. The nominal lattice constants for graphite are $a_G = 2.4589\text{\AA}$, $c_G = 6.674\text{\AA}$.[18] For reflectivity data we use unsubscripted reciprocal-space coordinates (h, k, ℓ) that refer to the standard substrate 4H-SiC hexagonal reciprocal lattice units that are rotated 30° from the graphite reciprocal lattice basis. The measured lattice constants were: $a_{\text{SiC}} = 3.0802 \pm 0.0006\text{\AA}$, $c_{\text{SiC}} = 10.081 \pm .002\text{\AA}$ for doped samples and $a_{\text{SiC}} = 3.0791 \pm 0.0006\text{\AA}$, $c_{\text{SiC}} = 10.081 \pm .002\text{\AA}$ for un-doped samples. These are within error bars of published values.[19]

RESULTS

To obtain detailed information about both the graphene films and the SiC-graphene interface, we have measured the surface x-ray specular reflectivity from graphitized 4H-SiC($000\bar{1}$). Specular reflectivity only depends on the momentum transfer perpendicular to the surface. The data is collected by integrating rocking curves [see Fig. 1(a)] around $q_{\parallel} = 0$ for different perpendicular moment transfer vectors, $q_{\perp} = 2\pi\ell/c_{\text{SiC}}$, where $\mathbf{q} = \mathbf{k}_f - \mathbf{k}_i$. Since the reflectivity only depends on q_{\perp} , the data can be analyzed using a one-dimensional model where all lateral information is averaged over the $0.4 \times 0.4\text{mm}$ x-ray beam. The scattered X-ray intensity $I(\Theta, q_{\perp})$ is then,

$$I(\Theta, q_{\perp}) = A(\Theta, q_{\perp})|F(q_{\perp})|^2, \quad (1)$$

where $F(q_\perp) = F(\ell)$ is the total scattering amplitude

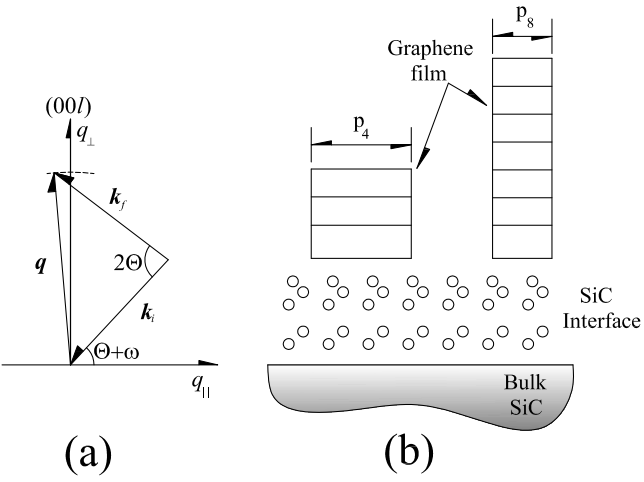


FIG. 1: (a) Schematic drawing of the reflectivity geometry. Incident wave \mathbf{k}_i strikes sample surface at an angle $\Theta+\omega$. The diffracted wave, \mathbf{k}_f , is kept fixed at 2Θ from \mathbf{k}_i . \mathbf{q} is "rocked" through the (00ℓ) rod by rotating the sample through an angle $\pm\omega$. (b) Model of multi-layer graphene islands grown on a SiC substrate with a reconstructed SiC interface layer. For specular reflectivity, all n -layers islands can be represented as one island with a fractional surface coverage parameter, p_n .

from the 4H-SiC substrate and the graphene film over layer. $A(\Theta, q_\perp)$ is a term that contains all corrections due to the experimental geometry. These include the Lorentz factor, footprint correction, effective sample area, polarization factor, and compensation for internal momentum transfer using critical wave vectors for both the substrate and the film.[20, 21] $F(\ell)$ is a coherent sum of the contributions from the graphene film and SiC substrate,

$$F(\ell) = e^{-2\gamma_{\text{SiC}} \sin^2 \pi\ell/m} \{F_{SiC}(\ell) + \frac{\rho_G}{\rho_{\text{SiC}}} F_G(\ell)\}. \quad (2)$$

ρ_{SiC} and ρ_G are the areal density of a 4H-SiC(0001̄) and a graphene (0001) plane, respectively. The weighting factor, $\rho_G/\rho_{\text{SiC}}=3.132$, properly normalizes the scattered amplitude from the graphene layer per 4H-SiC(0001̄) 1×1 unit cell. The exponential term in Eq. (2) is a roughness term that assumes c_{SiC}/m step fluctuations in the SiC surface (γ_{SiC} is approximately the probability of finding a step after traversing one SiC surface unit cell).[21] The step height is measured independently from measurements of the specular rod full width at half-maximum (FWHM) as a function of ℓ and gives the primary step height to be $c_{SiC}/2$.[6, 22]

To calculate $F_{SiC}(\ell)$ and $F_G(\ell)$ we use a model that has a SiC substrate reconstruction layer and allows for patches of the surface to be covered with different numbers of graphene layers. The schematic model of the graphene covered SiC is shown in Fig. 1(b). In the model the SiC substrate contribution is broken into two terms:

(i) the amplitude from a bulk terminated surface and (ii) the amplitude from a reconstructed SiC interface layer.

$$F_{SiC}(\ell) = \frac{F_{SiC}^{bulk}(\ell)}{1 - e^{-2\pi i \ell}} + F_{SiC}^I(\ell). \quad (3)$$

The first term in Eq. (3) is the bulk 4H-SiC structure factor, $F_{SiC}^{bulk}(\ell)$,[23] modified by the crystal truncation term, $(1 - e^{-2\pi i \ell})^{-1}$,[24]. The second term in Eq. (3), $F_{SiC}^I(\ell)$, is the structure factor of the reconstructed SiC surface. The SiC(0001) face is known to reconstruct into a 2×2 structure near the graphitization temperature.[25] However, the details of the reconstruction, and the nature of the SiC-graphene interface are not known. Although we cannot obtain lateral information about the interface structure from reflectivity data, the vertical shifts of atoms and layer density changes associated with them can be derived. To begin to understand this interface, we allow for a reconstruction by placing two SiC bilayers between the bulk and the multi-layer graphene film [Fig. 1(b)]. We then write the interface structure factor as:

$$F_{SiC}^I(q_\perp) = \sum_{j=1}^5 f_j \rho_j e^{-c_j^2 q_\perp^2} e^{iq_\perp z_j}, \quad (4)$$

where ρ_j is the relative atom density for the j^{th} interface layer ($\rho_j = 1$ for a bulk layer) at a vertical position z_j . f_j is the atomic form factor of C or Si. To allow for a reconstruction within each layer the term $\exp[-c_j^2 q_\perp^2]$ is added. The c_j 's are the rms vertical displacements of atoms due to a reconstruction in that layer.[26] The 5th layer is added to explore the possibility of adatoms between the SiC and the graphene.

To be completely general, we allow the scattered amplitude, $F_G(\ell)$, from the graphene film in Eq. (2) to take into account the possibility of a spatial distribution of varying graphene layers. This is done by defining an occupancy parameter p_n as the fractional surface area covered by all graphene islands that are n graphene layers thick. p_n is subject to the constraint equation $\sum p_n = 1$, where p_0 is the fraction of area that has no graphene. The multi-layer graphene structure factor can then be written in the general form:

$$F_G(\ell) = f_C \left(\sum_{n=1}^{N_{\max}} p_n e^{-q_\perp^2 \sigma_G^2 / 2} \sum_{m=1}^n e^{2\pi i l z_m / c} \right), \quad (5a)$$

$$z_m = \begin{cases} D_0 + (m-1)D_1 & m \leq 2 \\ D_0 + D_1 + (m-2)D_G & m > 2 \end{cases}. \quad (5b)$$

f_C is the atomic form factor for carbon and N_{\max} is the number of graphene layers in the highest island. The coordinates z_m in Eq. (5) are the position of the m^{th} graphene atomic layer relative to the last plane of SiC interface atoms. D_0 is the spacing between the bottom

layer of an island and the substrate and D_G is the average layer spacing between graphene layers in an island (see Fig. 2). We have allowed the spacing between the first and second layer graphene, D_1 , to be different from the bulk to allow for differences due to a different bonding geometry with the substrate. Because STM studies of multi-layer graphene films grown on the Si-face indicate some buckling of the graphite layer,[27] we also allow for a small vertical height distribution in each graphene layer. This is modelled similar to the interface relaxations in Eq. (4) by a Debye-Waller term, σ_G . As we will show, C-face graphene films show no significant buckling.

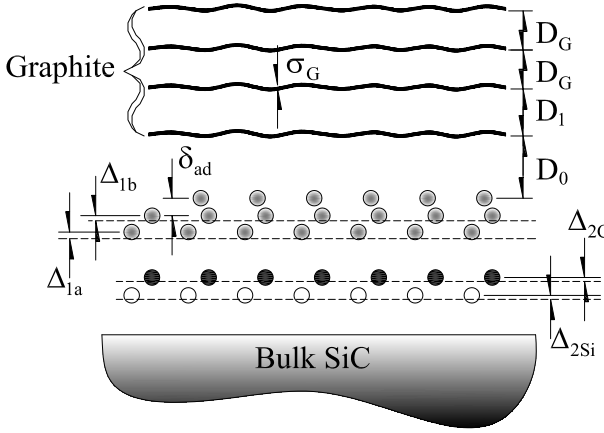


FIG. 2: A schematic model of multi-layer graphene grown on the 4H-SiC(000 $\bar{1}$) substrate. Dashed lines are the bulk SiC lattice planes before interface relaxation (Δ 's). The 5th (adatom) layer is displaced δ_{ad} from the last interface layer. (●) are carbon atoms and (○) are silicon atoms. The shaded circles in the top three layers of the interface can be either carbon or silicon atoms depending on which of the two models, Carbon-corrugated or Carbon-rich, is used.

Reflectivity data for a C-face multi-layer graphene film are shown in Fig. 3. The main bulk 4H-SiC peaks occur at $\ell = 4$ and $\ell = 8$. The sharp peaks at $\ell = 2$, 6 and 10 are the "quasi-forbidden" reflections of bulk SiC.[23] The graphite bulk reflections are expected at $\ell \sim 3$, 6 and 9. While there are many variables in Eqs. (1)-(5) that eventually must be fit, a number of the parameters are quite unique and insensitive to the exact structural model used for the SiC-graphene interface. For instance, because the graphite Bragg points are intense and narrow in ℓ , the mean spacing between graphene layers, D_G , is determined with high accuracy relative to the known SiC lattice constant. Similarly, the graphene layer roughness or corrugation, σ_G , is determined almost solely by the intensity decay of the graphite Bragg points as a function of ℓ . Once these nearly model-independent parameters are determined, they are fixed so that different structural models of the interface can be compared without relying on adjusting large numbers of parameters.

We have tested a number of structural models for the

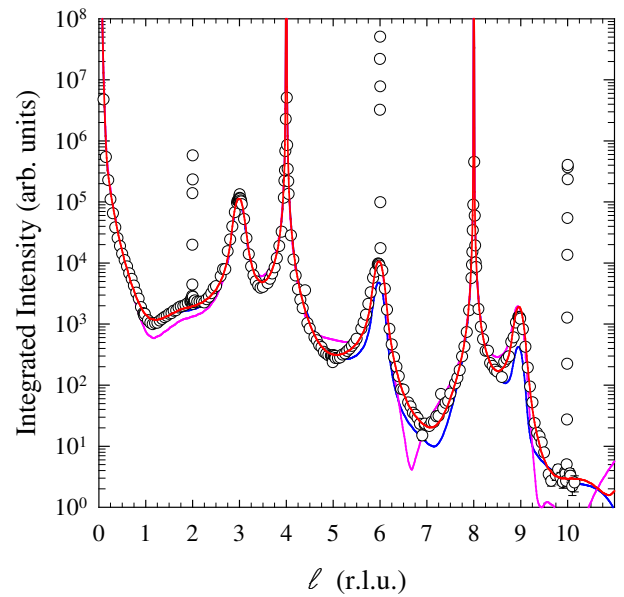


FIG. 3: Specular Reflectivity vs. q_\perp (in r.l.u.) for graphitized 4H-SiC(000 $\bar{1}$) C-face surface with 9 graphene layers. Solid lines are best fits to the structural models described in the text. Red solid line is the best fit to the structural model with a smooth graphene layer ($\sigma_G = 0.0\text{\AA}$). Blue solid line is the best fit with a corrugated graphite layer ($\sigma_G = 0.25\text{\AA}$). Magenta line is the best fit if the graphene substrate distance D_0 is reduced 10%.

graphene/4H-SiC(000 $\bar{1}$) interface. Simple relaxations of the top SiC bi-layers always give poor fits to the data. Even attempts to make a carbon rich phase that extends many layers into the bulk, a model that has been proposed in the literature[7, 28, 29], was not compatible with the data. The best fit model is a distorted bilayer between the graphene and bulk SiC. A schematic of the model is shown in Fig. 2. In this model the first bilayer above the bulk is slightly relaxed. However, the next bilayer (immediately below the graphene) has a significant relaxation. As we will show below, two similar versions of this model structure give nearly identical fits to the data.

Before looking at the details of these models, we point out a few important model-independent parameters for the graphite film. First, the average graphene inter-layer spacing is found to be $D_G = 3.368 \pm .005\text{\AA}$. This and other graphite film parameters are given in Table I. The value was determined from samples with films ranging from 9-13 graphene layers (averaged over the beam footprint). As mentioned above the inter-layer spacing is nearly independent of all other fit parameters and can be determined with high accuracy because it is fixed by the ℓ position of the three strong graphite Bragg peaks in Fig. 3. The inter-layer spacing is larger than bulk crystalline graphite (3.354\AA)[18] but smaller than the lattice spacing of turbostratic graphite ($D_{TG} = 3.440\text{\AA}$).[30, 31]

TABLE I: Structural parameters for graphene grown on 4H-SiC(0001) C-Face. Parameters are defined in Fig. 2

	D_0 (Å)	D_1 (Å)	D_G (Å)	σ_G (Å)
fit value	1.62	3.41	3.368	0.00
uncertainty	0.08	0.04	0.005	0.05

The larger spacing is due to stacking faults between adjacent layers caused by interference between π^* states that give rise to a larger repulsive interaction between adjacent graphene sheets.[30]

Another parameter that is insensitive to the details of the model is, σ_G , in Eq. (5a). This parameter can be interpreted two ways: either as a finite width of a graphene layer due to buckling of carbon atoms in the layer, or as an RMS roughness of a graphene layer due to vertical disorder over the coherence length of the x-ray beam ($\sim 2\mu\text{m}$). We find that $\sigma_G = 0.0 \pm 0.05\text{\AA}$ (see Table I). Because of the exponential form in Eq. (5a), a finite layer width manifests itself as a rapid decay in the graphite Bragg peak intensity at high ℓ . This is demonstrated in Fig. 3 where we compare a flat graphite film to a film with an RMS thickness of $\sigma_G = 0.25\text{\AA}$. The finite layer width severely reduces the graphite peak intensities at $\ell = 6$ and 9.

Fits to the reflectivity show that two similar model structures for the interface region between the bulk and the graphene represent the experimental data equally well. We refer to these models as the "Carbon-corrugated" and "Carbon-rich" models. In both models the SiC bilayer immediately above the bulk in Fig. 2 remains "bulk-like" in terms of both density and inter-layer spacing. The two models are distinguished by the structure of the next three layers just below the graphene film. Ball models of the two structures are shown in Fig. 4 and the detailed fitting parameters are given in Table II. Structural values were determined for three different samples. The fitting parameter variations from sample to sample are included in the uncertainty limits of Table II.

In the C-Corrugated model the last SiC bilayer is contracted inwards towards the bulk by 0.11\AA to give a slightly smaller Si–C bond length. In the uppermost bilayer the carbon is buckled into two equal density layers. The density of both the Si layer (ρ_{1a}) and the sum of the buckled carbon layers ($\rho_{ad} + \rho_{1b}$) in this bilayer are each $\sim 2/3$ of the bulk value. It is unlikely that the last layer is a carbon adatom. If it were, the density required to saturate the dangling bonds in the carbon layer below would be $\rho_{ad} = \rho_{1b}/3$ instead of being equal. For this reason we refer to the model as a corrugated surface. We note that the fits are very sensitive to the Si density, ρ_{1a} , in the last bilayer. If we force the last bilayer to have the same Si atom density as in the bulk, the best fit model cannot reproduce the data. This is demonstrated in Fig. 5 where we show a best fit to

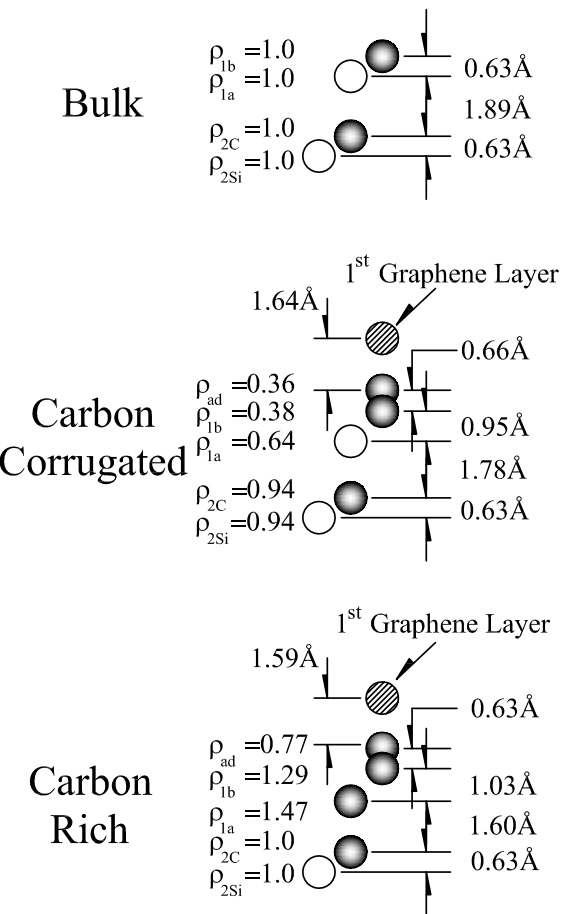


FIG. 4: Schematic ball models of bulk, C-Corrugated and C-Rich interface layers between the substrate and the graphene film. (●) are carbon atoms and (○) are silicon atoms. Hatched atoms are carbon atoms in the first graphene layer. Interlayer spacings and densities (relative to bulk SiC) are shown.

the "C-Corrugated" model but force ρ_{1a} to be the bulk density. Similarly, removing the buckling in the carbon layer ("Smooth C-layer" model) while keeping the total density the same cannot reproduce the reflectivity modulation between $0.5 < \ell < 2.5$ (see Fig. 5).

To first order the ratio of the atomic form factors for Si and C, f_{Si}/f_C in Eq. (4), are determined simply by the ratio of their atomic numbers $14/6 = 2.33$. Therefore, the model calculation should give a similar fit if the Si atoms in the top SiC bilayer are replaced by carbon atoms with 2.33 times the density ($\sim 2.33 \times 0.64 = 1.49$). This replacement gives the "C-rich" model shown in Fig. 4 with densities and layer spacings adjusted to give the best fit to the data. In Fig. 4 the best fit parameters show that there are two main differences between the C-Corrugated and C-Rich models. First, the layer spacings between bi-layers is considerably shorter (1.60\AA) and second, the densities in the last layers are higher. The bilayer spacing measured in the C-rich model is slightly larger than the

TABLE II: Best-fit interfacial structural parameters for graphite covered 4H-SiC(000 $\bar{1}$) (C-Face). Data for both the "C-Corrugated" and "C-Rich" models give nearly identical fits. All fits find $c_j \sim 0\text{\AA}$ for all layers. Parameters are defined in Fig. 2

	δ_{ad} (\text{\AA})	ρ_{ad} (\text{\AA})	Δ_{1b} (\text{\AA})	ρ_{1b} (\text{\AA})	Δ_{1a} (\text{\AA})	ρ_{1a}	$\Delta_{2C} = \Delta_{2Si}$ (\text{\AA})	$\rho_{2Si} = \rho_{2C}$
C-corrugation	0.66	0.36	0.18	0.38	-0.14	0.64	-0.03	0.94
Atom Type		carbon		carbon		silicon		
C-rich	0.63	0.77	0.11	1.29	-0.33	1.47	-0.04	0.94
Atom Type		carbon		carbon		carbon		
uncertainty	0.04	0.08	0.04	0.08	0.04	0.10	.04	.05

bond length of diamond (1.54\AA).[32] The higher carbon layer densities have a similar significance in that they lie half way between the SiC density ($\rho = 1.0$) and that of graphene ($\rho = 3.13$). In fact, the first C-layer in the bilayer has a density close to the atom density of a (111) diamond plane, 1.51.

While it may seem reasonable to expect that as Si sublimates from the surface a carbon rich interface forms with some diamond-like character, we should caution that there are other ways to interpret these results. First of all, the spacing between planes in the bilayer is much larger, $0.63\text{--}1.03\text{\AA}$, while in diamond they should be much lower, 0.51\AA . The C-Rich phase is also considerably different from the "extended diamond phase" proposed in the literature because it does not extend beyond the first bilayer.[7, 28, 29] In both models the relaxation of the bilayer above the bulk is small, contrary to what might be expected if there were significant density changes in that layer. These small changes from the model are not due to an insensitivity to either the layer spacings or the layer density. This is shown in Fig. 6 where we compare calculated best-fit reflectivities when either the Si density ρ_{2Si} is reduced or the Si–C spacing Δ_{2Si} is changed from the ideal value. As can be seen, interplanar spacing changes of less than 5% ($< 0.1\text{\AA}$) lead to obviously poor fits. Similarly, reducing the Si atom density in this layer by more than 25% makes the fit much worse. Therefore, the interfacial layer does not extend much beyond the top-most SiC bilayer. Note also that the total layer density of the last three interface layers is $\rho = 1.47 + 1.29 + 0.77 = 3.53$. This density is slightly larger than the density of a graphene sheet ($\rho = 3.13$). Rather than thinking of this layer as an ideal diamond like layer, it may be more appropriate to view it as a buckled graphene sheet with a mixture of sp^2 and sp^3 bonded carbon.

The most important finding from this work is that the first graphene layer sits above the last bulk carbon layer at a distance of $D_0 = 1.62 \pm 0.08\text{\AA}$. This value is, within error bars, insensitive to which structural model is used and can be determined with reasonable sensitivity as demonstrated in Fig. 3. The figure shows that 10% variations in D_0 from its optimal value lead to very poor fits to the data. The very short bond distance measured sug-

gests that the first graphene layer is not simply bonded to the substrate with Van der Waal's bonds but instead has a much stronger interaction with the substrate.

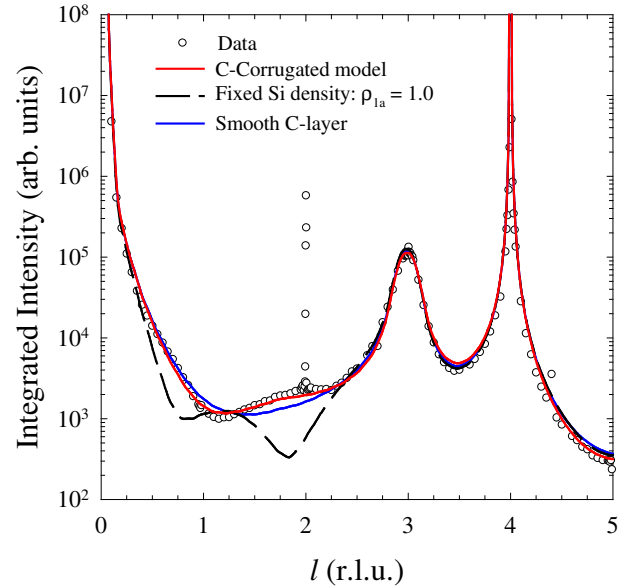


FIG. 5: Specular Reflectivity for graphitized 4H-SiC(000 $\bar{1}$) C-face surface. (o) are the data. Red line is the best fit to the Carbon-corrugated top layer. The black dashed line show the fit for the same model if the Si layer density is fixed at the bulk value ($\rho_{1a} = 1$). The blue line is a fit when the carbon corrugation in the top layer is removed but the total density remains the same ("Smooth C-layer").

DISCUSSION

The x-ray reflectivity data shows that the interface between epitaxial graphene and the 4H-SiC(000 $\bar{1}$) substrate is sharp. The interface is comprised of no more than 1–2 SiC bi-layers. The graphene that grows is flat (i.e. $\sigma_G = 0\text{\AA}$) except for a small potential buckling of the first layer. There are two key structural parameters that deserve attention. The first is the inter-layer spacing between graphene sheets that is much larger than expected for $AB\dots$ stacked graphene layers and points to

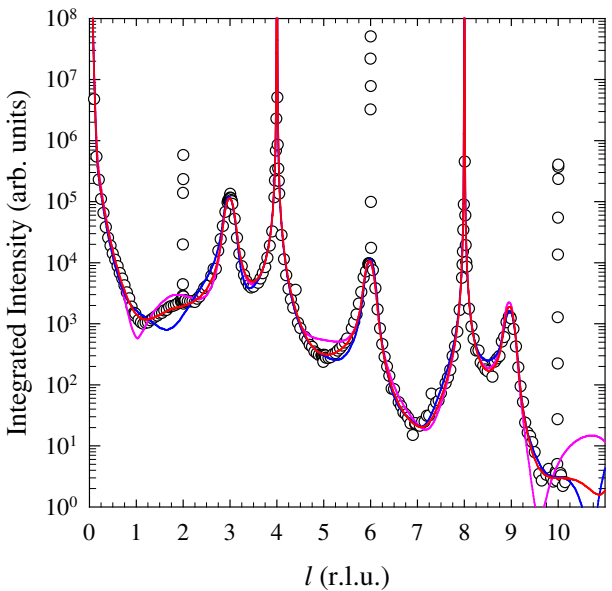


FIG. 6: A comparison of the calculated reflectivity vs. q_{\perp} (in r.l.u.) for different first bilayer models. Red line is the best fit structure with bulk bilayer parameters. Blue line is a fit with ρ_{2Si} fixed at a value 25% less than the bulk. Magenta line is a best fit with the both Δ_{2Si} and Δ_{2C} relaxed towards the bulk by 5%.

a significant stacking fault density in the film. Because stacking faults cause interference between π^* states in adjacent layers, these layers have a larger spacing. The mean layer spacing can, therefore, be used to estimate the stacking fault density.[30] If we define the probability, γ , that any two adjacent sheets are faulted, then the inter-layer spacing will range from that of $AB\dots$ stacked graphite (3.354\AA) when $\gamma = 0$ to that of turbostratic graphite (3.44\AA) when $\gamma = 1$. In that case the average inter-layer spacing for some finite number of stacking faults is approximately;[30]

$$D_G = 3.44 - 0.086(1 - \gamma^2). \quad (6)$$

Using the measured $D_G = 3.368\text{\AA}$, gives $\gamma = 0.4$ for these C-face films. In other words, after every $1/(1 - \gamma) = 1.6$ graphene sheets, a stacking fault occurs in the film. The fact that there are frequent stacking faults is not surprising since there is significant rotational disorder of graphene layers grown on this surface.[6, 8] A pair of graphene sheets that are rotated with respect to each other would lead to regions of local $AB\dots$ stacking separated by regions with other stacking arrangements. The mean graphite inter-layer spacing would then be determined by the degree of rotational disorder. Experiments to quantify the stacking and rotational disorder are currently underway.

The existence of a large stacking fault density has an important bearing on the results of conductivity experiments on C-face grown multi-layer graphene films.

Magnetotransport [5], Infared Spectroscopy (IRS) [36] and photoemission experiments [12] indicate that multi-layer graphene films grown in SiC behave like isolated graphene sheets. In the photoemission experiments a clear Dirac dispersion cone is measured. The origin of this type of dispersion in the electronic band structure is the symmetry of carbon bonding in a single graphene sheet. $AB\dots$ stacking in multi-layer graphene films (i.e graphite stacking) would break that symmetry and causes significant changes to the band structure, even for a few layers.[13, 14] In the multi-layer graphene films grown on the C-face of SiC, the $AB\dots$ stacking disorder may inhibit symmetry breaking and allow sheets in the film to behave electronically as if they were physically isolated.[14]

In addition to the stacking fault density, the short bond length, D_0 , between the interface and the first graphene sheet indicates an additional way the graphene sheets become isolated from the substrate. While the $AB\dots$ stacking in bulk graphite breaks the hexagonal symmetry of an isolated graphene sheet, it has been assumed that the substrate-graphene interaction will have a similar effect.[14] Indeed the short D_0 bond length measured here for the graphene/4H-SiC(0001) interface implies a strong interaction that is consistent with Photoemission results.[8] The short bond length we measure for the C-face films has been recently confirmed by *ab-initio* calculations.[15] Those calculations show that when a single graphene layer is grown on a SiC substrate the material remains insulating. The Dirac cone dispersion, of an isolated graphene sheet does not appear until a second graphene layer is formed.[15] Therefore, the first carbon layer with a graphene density acts like a "buffer" layer between the substrate and the rest of the graphene film. From the structural properties of the graphene/SiC interface measured here, a model emerges that may explain the graphene character of these films seen in magnetotransport, IRS, and Photoemission measurements as well as in band structure calculations. In this model, one or two graphene layer, primarily responsible for the conduction, lies between the "buffer" layer and the imperfectly stacked graphene layers above it.

While the nature of the buffer layer is not completely characterized, the reflectivity data offer two possibilities. (1) In the C-Corrugated model the buffer layer is simply the first flat graphene layer above the interface. The SiC bilayer below this layer is relaxed with a lower density of atoms compared to the bulk. (2) In the C-rich structure, a highly buckled carbon layer, with a total carbon density nearly equal to graphene, resides between the substrate and the rest of the film. Low Energy Electron Diffraction (LEED) experiments show that UHV-grown multi-layer graphene on the C-face surface exhibits a 2×2 reconstruction.[25] Our x-ray measurements confirm that a 2×2 structure still persists even when the films are thick enough that LEED is no longer capable of prob-

ing the interface.[6] The long range order of the 2×2 reconstruction is $\sim 200\text{\AA}$. This is much smaller than the film structural coherence length of $\sim 3000\text{\AA}$ and suggests that the interface is never fully ordered. A possible explanation maybe that different parts of the surface are in different stages of graphitization.

It is significant that the RMS layer width of the graphene is zero, σ_G in Eq. (5a). σ_G can represent either a random film roughness or a RMS corrugation of the graphene that is commensurate with the substrate. Because it is zero, we can conclude that beyond the buffer carbon layer the graphene layers are flat and must be very weakly interacting with any substrate potential. This explains why C-face graphene films can be rotationally disordered but have large domain sizes. The energy cost per atom to rotate a graphene sheet on a flat graphene substrate is very low ($< 50\text{meV/atom}$).[33, 34] At the growth temperatures of 1400°C , and given the low registry forces implied from these experiments, growing graphene sheets can rotate freely, rather than becoming polycrystalline as suggested by Forbeaux et al.[8] On Si-face multi-layer graphene films the situation is different. There is a $(6\sqrt{3} \times 6\sqrt{3})R30^\circ$ reconstruction in the first 2-3 graphene layers on this surface.[7, 35] The graphene has a nonzero corrugation of about 0.25\AA [27] that could be enough to lock the growing film into registry. Step boundaries or other defects in the substrate can put domain boundaries in the graphene that are not easily removed by rotating large areas of the film.

SUMMARY

In this work we have measured a number of important structural parameters of multi-layer graphene grown on the carbon terminated $4\text{H-SiC}(000\bar{1})$ surface. The most important finding is that the separation between the first graphene layer and the SiC surface is very short (1.62\AA). This distance is not much larger than a diamond bond length implying a very strong interaction between the first graphene layer and the substrate. It is consistent with recent band structure calculations that show a large energy gap for a single graphene layer on the $4\text{H-SiC}(000\bar{1})$ surface.[15] Subsequent graphene layers have an RMS corrugation (averaged over 9 layers) that is less than 0.05\AA . This suggest that the strongly bound buffer graphene layer shields subsequent layers from the interface corrugation potential. Therefore, unlike exfoliated graphene flakes deposited on SiO_2 [16], the graphene layers grown by sublimation on the C-face of SiC are very smooth.

The graphene films show evidence of a large density of stacking faults. While the topography of these faults remains to be determined, it does suggest that the $AB\dots$ stacking of bulk graphite is not present in these films. This may be the reason why Dirac electrons, expected

only in isolated graphene sheets where $AB\dots$ stacking does not break the graphene symmetry, are seen in this multi-graphene system.

Acknowledgments

This research was supported by the National Science Foundation under Grant No. 0404084, and by Intel Research. The Advanced Photon Source is supported by the DOE Office of Basic Energy Sciences, contract W-31-109-Eng-38. The μ -CAT beam line is supported through Ames Lab, operated for the US DOE by Iowa State University under Contract No.W-7405-Eng-82. Any opinions, findings, and conclusions or recommendations expressed herein are those of the authors and do not necessarily reflect the views of the research sponsors.

References

- [1] C. Berger, Z. Song, T. Li, X. Li, A.Y. Ogbazghi, R. Feng, Z. Dai, T. Grenet, A.N. Marchenkov, E.H. Conrad, P.N. First, W.A. de Heer, *J. Phys. Chem. B* **108**, 19912 (2004).
- [2] K.S. Novoselov, A.K. Geim, S.V. Morozov, D. Jiang, M.I. Katsnelson, I.V. Grigorieva, S.V. Dubonos and A.A. Firsov, *Science* **306**, 666 (2004).
- [3] K.S. Novoselov, A.K. Geim, S.V. Morozov, D. Jiang, M.I. Katsnelson, I.V. Grigorieva, S.V. Dubonos and A.A. Firsov, *Nature* **438**, 197 (2005).
- [4] Y. Zhang, Y.-W. Tan, H.L. Stormer and P. Kim, *Nature* **438**, 201 (2005).
- [5] C. Berger, Z. Song, X. Li, X. Wu, N. Brown, C. Naud, D. Mayou, T. Li, J. Hass, A.N. Marchenkov, E.H. Conrad, P.N. First and W.A. de Heer, *Science* **312**, 1191 (2006).
- [6] J. Hass, R. Feng, T. Li, X. Li, Z. Song, W.A. de Heer, P.N. First, E.H. Conrad, C.A. Jeffrey, and C. Berger, *J. Appl. Phys. Lett.* **89**, 143106 (2006).
- [7] A.J. Van Bommel, J.E. Crombeen, and A. Van Tooren, *Surf. Sci.* **48**, 463 (1975).
- [8] I. Forbeaux, J.-M. Themlin, A. Charrier, F. Thibaudeau, and J.-M. Debever, *Appl. Surf. Sci.* **162/163**, 406 (2000).
- [9] A. Charrier, A. Coati, T. Argunova, F. Thibaudeau, Y. Garreau, R. Pinchaux, I. Forbeaux, J.-M. Debever, M. Sauvage-Simkin, and J.-M. Themlin, *J. Appl. Phys.* **92**, 2479 (2002).
- [10] M. Kusunoki, T. Suzuki, T. Hirayama, N. Shibata, and K. Kaneko, *Appl. Phys. Lett.* **77**, 531 (2000).
- [11] T. Angot, M. Protail, I. Forbeaux and J.M. Layet, *Surf. Sci.* **502-503**, 81 (2002).
- [12] E. Rollings, G.-H. Gweon, S. Y. Zhou, B. S. Mun, J. L. McChesney, B. S. Hussain, A. V. Fedorov, P. N. First, W. A. de Heer, A. Lanzara, *J. Phys. and Chem. of Solids* **67**, 2172 (2006).

- [13] E. McCann and V. I. Fal'ko, *Phys. Rev. Lett.* **96** 086805 (1996).
- [14] S. Latil and L. Henrard, *Phys. Rev. Lett.* **97**, 036803 (2006).
- [15] F. Varchon, R. Feng, J. Hass, X. Li, B. Ngoc Nguyen, C. Naud, P. Mallet, J.-Y. Veuillem, C. Berger, E.H. Conrad and L. Magaud, arxiv.org/abs/cond-mat/0702311 (2007).
- [16] S.V. Morozov, K.S. Novoselov, M.I. Katsnelson, F. Schedin, L.A. Ponomarenko, D. Jiang, and A.K. Geim, *Phys. Rev. Lett.* **97**, 016801-1 (2006).
- [17] Cree Inc., 4600 Silicon Drive, Durham, NC 27703.
- [18] Y. Baskin and L. Mayer, *Phys. Rev.* **100** 544 (1955).
- [19] A. Bauer, J. Kräusslich, L. Dressler, P. Kuschnerus, J. Wolf, K. Goetz, P. Käckell, J. Furthmüller and F. Bechstedt, *Phys. Rev.* **B57** 2647 (1998).
- [20] I.K. Robinson in; *Handbook on Synchrotron Radiation*, Vol. 3, eds. G.S. Brown and D.E. Moncton, (North-Holland, Amsterdam, 1991) p.221.
- [21] R. Feng, Ph.D. Thesis, Georgia Institute of Technology (2006).
- [22] see for example, E.H. Conrad in: *Handbook of Surface Science* ed. N.V Richardson and S. Holloway, Vol. **1** p271-360 (Elsevier, Amsterdam, 1996).
- [23] A. Bauer, Ph Reischauer, J. Kräusslich, N. Schell, W. Matz and K. Goetz, *Acta Cryst. A* **57**, 60 (2001).
- [24] I.K. Robinson, *Phys. Rev.* **B33** 3830 (1986).
- [25] I. Forbeaux, J.-M. Themlin, and J.-M. Debever, *Surf. Sci.* **442**, 9 (1999).
- [26] I.K. Robinson and E. Vlieg, *Surf. Sci.* **261**, 123 (1992).
- [27] T. Li, Ph.D. Thesis, Georgia Institute of Technology (2006).
- [28] I. Forbeaux, J.-M. Themlin, and J.-M. Debever, *Phys. Rev. B* **58**, 16396 (1998).
- [29] N. Barrett, E.E. Krasovskii, J.-M. Themlin, V.N. Strocov, *Phys. Rev. B* **71**, 035427 (2005).
- [30] R.E. Franklin, *Acta Cryst.* **4**, 253 (1951).
- [31] L. G. Cançado, M. A. Pimenta, R. Saito, A. Jorio, L. O. Ladeira, A. Grüneis, A. G. Souza-Filho, G. Dresselhaus, and M. S. Dresselhaus, *Phys. Rev. B* **66**, 035415 (2002).
- [32] J.K. Burdett in *Chemical Bonding in Solids* (Oxford University Press, New York, 1995) p.152.
- [33] L.A. Girifalco and R.A. Ladd, *J. Chem. Phys.*, **25** 693 (1956).
- [34] A.N. Kolmogorov and V.H. Crespi, *Phys. Rev.*, **B 71** 235415 (2005).
- [35] T. Tsukamoto, M. Hiria, M. Kusaka, M. Iwami, T. Ozawa, T. Nagamura, and T. Nakata, *Surf. Sci.* **371**, 316 (1997).
- [36] M.L. Sadowski, G. Martinez, M. Potemski, C. Berger, and W.A. de Heer, *Phys. Rev. Lett.* **97** 266405 (2006).